Available online at www.sciencedirect.com

ScienceDirect

Journal of the European Ceramic Society 34 (2014) 2509–2517

www.elsevier.com/locate/jeurceramsoc

Yttria nettings by colloidal processing

S.C. Santos [a,*], W. Acchar [b], C. Yamagata [a], S. Mello-Castanho [a]

[a] Center of Materials Science and Technology, Nuclear and Energy Research Institute – IPEN, 2242 Lineu Prestes Avenue, University City, São Paulo, Brazil
[b] Federal University of Rio Grande do Norte – UFRN, University Camp of Lagoa Nova, Rio Grande do Norte, Natal, Brazil

Received 30 September 2013; received in revised form 5 March 2014; accepted 10 March 2014
Available online 27 March 2014

Abstract

Porous ceramic burners have been shown as a promising technology to produce heat and lighting by burning low calorific fuels like modern biomass. Among ceramics, yttria (Y_2O_3) presents considerable luminescent proprieties for gas burner technology. By colloidal processing of yttria, this work aims to produce luminescence ceramic nettings with potential to be used as gas burners. Processing parameters such as mean particle size, zeta potential and flow behavior were evaluated in order to prepare suitable suspensions for replica method. Yttria nanoparticles presented light emission with $\lambda = 550$ nm when being thermal stimulated at 150 °C. Besides, the nano sized powders $d_{50} = 113.8$ nm and specific surface area of 13.6 $m^2\ g^{-1}$ could be highly stabilized at pH 10.5. Suspensions with 30 vol% of solids, pH 10.5, 1 wt% of dispersant and 0.3 wt% of binder presented shear thinning behavior and thixotropy suitable for replica method. As a result, samples sintered at 1600 °C/1 h showed homogeneous morphology of struts and porous microstructure desirable for gas recirculation and burning process.

Keywords: Yttria; Ceramic processing; Porous ceramic; Gas burners; Luminescence

1. Introduction

Yttria (Y_2O_3) is one of the most important rare earth oxides. This structure is generally referred to as C-type. According to Hoekstra et al.[1] all the rare earths sesquioxides belong to this system such as Dy_2O_3, Th_2O_3, Ga_2O_3 and In_2O_3. Nevertheless, three Y_2O_3 polymorphs have been found. Gourlaouen et al.[2] and Srikanth et al. reported the monoclinic structure (B-type) at 997 °C under 2.0 GPa during plasma spray coating. Navrotsky et al.[3] showed that the C-type becomes fluorite type at 2308 °C and hexagonal A-type at 2325 °C. Quin et al.[4] observed structural changes from C-type to B-type for yttria nanoparticles smaller than 10 nm. Yttria has similar chemical and physical proprieties to other rare earth elements, thus is very used as matrix to compose luminescence materials. Wang et al.[5] reported that lighting emission of Y_2O_3:Eu^{3+} increased as a function of crystallite size and particle. Zhang et al.[6] observed a significant emission improvement for Y_2O_3:Eu^{3+} phosphors as synthesized by combustion reaction as well as sintering in vacuum. Goldburt et al.[7] described that Y_2O_3:Tb phosphors with particle diameter of 10 Å presented higher emission than those with 100 Å. Furthermore, Y_2O_3 is a potential material to be used in porous burners for lighting.

Barrer et al.[8] found out that lighting emission by gas combustion in porous components was more efficient rather than a free flame. The porous structure works as heat circulator, which improves flame speed, stability and low emission of CO_2. Thus, this technology fulfills requirements on lower pollution emissions (NO_x, CO), according to United Nations' Low Carbon plans.[9]

The processes commonly applied to produce porous ceramic components are sacrificial template, gel casting and replica.[10] The last one is very useful due to its applicability for any ceramic material dispersed in suspension. Further, the template can be any organic material to be burned out during thermal treatment. Several materials have been used such as wood,[11] carbon sponge,[12] polyurethane foam,[13] vegetal sponge,[14] coral mineral,[15] coral skeletal carbonate,[16] echinoid spines.[17]

* Corresponding author at: Center of Materials Science and Technology, Nuclear and Energy Research Institute – IPEN, 2242 Lineu Prestes Avenue, 05508-000 University City, São Paulo, Brazil. Tel.: +55 11 31339207/200; fax: +55 11 31339201.
E-mail addresses: silas.cardoso@usp.br, silascs@ipen.br (S.C. Santos).

http://dx.doi.org/10.1016/j.jeurceramsoc.2014.03.006
0955-2219/

By replica components with complex shape can be produced. However, the ceramic suspension has to present a suitable rheological behavior, wherein viscosity plays an important role during the processing. High viscosity suspensions are not desired, seeing that they present much resistance to flow. As a result, they cannot recover and enter into cavities of porous template either. On the other hand, low viscosity suspensions cannot remain on the surface of the template, since they flow easily. Thus, the ceramic suspension has to be able to flow while is subjected of external force and has to present higher viscosity as static condition. This flow characteristic is reported as shear thinning behavior.[18] In addition, thermal treatment is extremely important. Controlling the heating rate and temperature slope the organic template can be burned out without disrupt the ceramic structure.

Nowadays, few studies about colloidal processing of yttria have been reported. One of the first papers reporting the isoelectric point (IEP) of yttria was done by Moreno et al.[19] In this study was reported that the isoelectric point of yttria particles was located at pH 8.5 and the highest zeta potential value was achieved at pH 11 ($\zeta = |50\,\text{mV}|$). Fuji et al.[20] evaluated the stability of yttria suspensions as a function of dispersant concentration and pH. As a result, yttria suspensions prepared with 1 wt% of polyacrylic ammonium acid (PAA) showed the lowest viscosity. Li et al.[21] showed that stable YAG ($Y_3Al_5O_{12}$) aqueous slurry presented a minimum viscosity in pH range between 9 and 11. Santos et al.[22] determined that high stable yttria suspensions ($\zeta = |56\,\text{mV}|$) could be prepared at pH 10 and with 1 wt% of PAA. Sonoda et al.[22] reported that Y-doped CeO_2 suspensions were more stable in acid pH range rather than alkaline. By colloidal processing of yttria since powder characterization and conditioning until rheological evaluation, this study aims to determine suitable processing parameters to produce luminescent ceramic nettings with potential for gas burner technology.

2. Experimental

Yttria powder (Y_2O_3) supplied by Johnson Matthey. Firstly, the powders were subjected of milling in atritor mill for 1 h based on prior work.[23] Powder characterization was performed by helium pycnometry (Pycnometer Micrometrics 1330); scanning electron microscopy (SEM, Philips XL30); X-ray fluorescence (XRF, Rigaku RIX 3000); X-ray diffraction (XRD, Rigaku Multiflex), with scanning at 1°/min, range from 10 to 80° (2θ), radiation Cu-kα; thermal gravimetric and thermal differential analyses (TGA/TDA, Setaram S60/38336), with a heating rate of 10 °C/min up to 1400 °C, in ambient atmosphere and having alumina as reference material; Photon Correlation Spectroscopy (PCS, ZetaPALS Analyzer, Brookhaven Instruments) to determine particle size distribution. For PCS, diluted aqueous suspensions with 0.001 vol% of particles were prepared at pH 10.5 by adding NaOH solution (0.5 M). Before measurements samples were homogenized in ultrasonic cleaner for 30 min (optimized time); specific surface area, by BET method (SSA, Micrometrics ASAP 2010). In addition to SSA, theoretical mean particle diameter (d_{BET}) was determined by BET equation (Eq. (1)), which considers particles having homogeneous morphology. Besides, based on d_{BET} result was calculated the agglomeration factor (F_{ag}) as shown in Eq. (2).

$$d_{BET} = \frac{6}{\rho_t . S_M}[\mu\text{m}] \quad (1)$$

where d_{BET} = theoretical mean particle diameter (μm); ρ_t = theoretical density (g cm^{-3}); S_M = specific surface area (m^2 g^{-1}).

$$F_{ag} = \frac{d_{50}}{d_{BET}} \quad (2)$$

where d_{50} = experimental mean particle diameter (μm); d_{BET} = theoretical mean particle diameter (μm).

The emitted luminescence of yttria particles was measured by a combined thermoluminescence reader (model Risø TL/OSL-DA-20) based on a heating system up to 700 °C and spectrometer (Ocean Optics, model QE65 Pro) with spectral sensibility from 200 to 950 nm. The samples were heated with a heating rate of 2 °C/s until 400 °C in room atmosphere. Afterwards, the samples were cooled by a nitrogen flow until room temperature.

The stability of powders in aqueous medium was evaluated by measuring the electrophoretic mobility of the particles and determining zeta potential (ζ) using Smoluchowski model (Eq. (3)) and zetameter based on light phase scatter analyzing (ZetaPALS, Brookhaven Instruments Corporation, USA). Stock suspensions with 0.5 g L^{-1} of solids were prepared, having NaCl 10^{-2} M as indifferent electrolyte. HCl and KOH solutions were used to shift pH of stock suspensions from acid to alkaline (pH 5.6–12). In order to compare the effectiveness of dispersant dosage on stability concentrations from 0.5 to 2 wt% of polyacrylic ammonium acid (PAA, Duramax D3005, Rohm and Haas Co.) were added in stock suspensions. Before measurements, all suspensions were homogenized in ultrasound cleaner for 2 min.

$$\xi = \frac{\mu_e \eta}{\varepsilon}[\text{mV}] \quad (3)$$

where ε = permittivity of liquid (J/V^2 m); η = viscosity of liquid (cP); μ_e = electrophoretic mobility of particles (μ s^{-1} V^{-1} cm).

Yttria aqueous suspensions were prepared varying solids loading from 15 to 33 vol% and using the following additives PAA, tetramethylammonium hydroxide (TMAH, Sigma–Aldrich) and carboxymethyl cellulose (CMC, Sigma–Aldrich) from 0.3 to 1 wt% (based on suspension weight). All suspensions were homogenized by ball milling for 24 h with alumina balls ($\varnothing_{balls}$ = 10 mm).

The flow behavior of suspensions was performed by a rheometer (Haake RS600, Thermo Scientific, Germany). The sensor system consisted in a double cone rotor and a stationary plate (DC60/1°). The characterization was carried out by flow curves in controlled rate mode (CR). Measurements were performed at 25 °C by increasing the shear rate from 0 to 1000 s^{-1} in 5 min, holding at 1000 s^{-1} for 2 min and returning to 0 s^{-1} in 5 min. For each CR run 200 points were measured.

For replica conformation a cotton-nylon netting (CNT) was selected as template considering its cells morphology distribution. Samples of CNT were immersed into yttria suspension; afterwards the excess of suspension was removed by squeezing

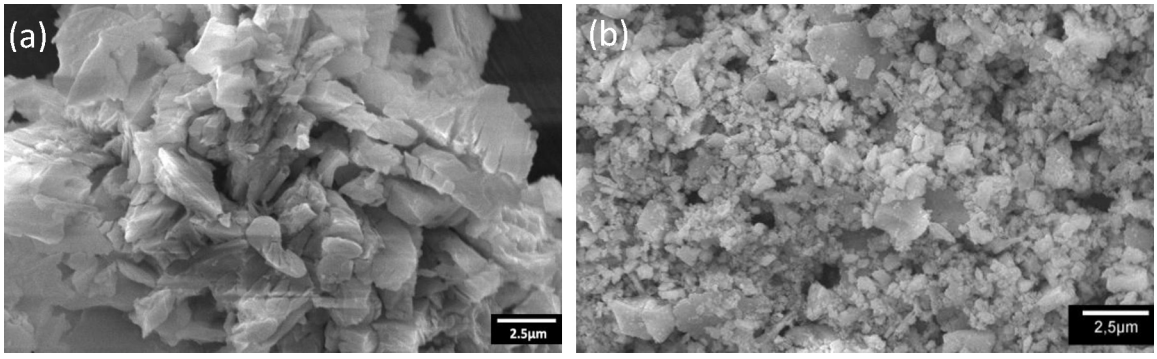

Fig. 1. Micrographs of yttria powders by SEM (a) as received and (b) after milling for 1 h.

out the samples. After drying in ambient temperature for 24 h, impregnated CNT samples were sintered at 1600 °C/1 h in ambient atmosphere by vertical furnace (Lindberg/Blue M). Densities of sintered samples were determinate by Helium Pycnometry and surface microstructure evaluated by stereoscope (Jena GSZ, Carl Zeiss) and SEM.

3. Results and discussion

Fig. 1 shows micrographs by scanning electron microscopy (SEM) of Y_2O_3 powders as received and after milling for 1 h. Before processing Y_2O_3 presented board shape agglomerates of particles larger than 2 μm. On the other hand, milling for 1 h was able to break down the agglomerates into smaller particle size distribution, which is desirable for preparing stable and concentrated suspensions. In our previous work, we evaluated the milling time of yttria powders by atritor mill from 1 to 5 h. As consequence, the first hour of processing was the most efficient, reducing particle size from d_{50} = 6.51 μm to d_{50} = 1.53 μm and for 3 h from 1.53 μm to 1.31 μm. However, for 5 h the milling was not effective anymore d_{50} =1.31 μm to d_{50} = 1.52 μm. Furthermore, after 3 h of processing particles started agglomerating.

Equivalent particle diameter by PCS of Y_2O_3 powders after milling is shown in Fig. 2. As a result, Y_2O_3 powders consists in a narrow nano sized particle distribution with a mean diameter (d_{50}) of 131.8 nm. Besides, the size difference (Span) between minor (d_{10}) and major (d_{90}) distributions was only 1 nm. Furthermore, relating span to d_{50} (relative span) this difference is much less 0.01. Therefore, Y_2O_3 showed a monomial distribution of particles.

The X-ray diffraction pattern (XRD) of Y_2O_3 powders is shown in Fig. 3. As a result, it agrees well with C-type cubic structure presenting high intensity pick around 29° according to powder diffraction file (P.D.F. 25-1200). No impurity peaks and no transition to monoclinic phases were observed, which indicates that the powders are pure in both chemistry and crystalline phase.

As result of X-ray fluorescence (XRF) of yttria powders, the sample showed Y_2O_3 (98.7 wt%), SO_3 (1.2 wt%), Fe_2O_3 (0.09 wt%), CuO (0.03 wt%). As the impurities concentration was less than 2 wt% it is not expected significant effect on dispersion of yttria particles. For colloidal processing, chemical composition of material is an important parameter, since impurities can influence positive or negatively on the stability of particles (electrophoretic mobility, zeta potential, isoelectric point).

Fig. 4 shows TGA/DTA results of Y_2O_3 powders. For temperature range until 1200 °C no exothermic peaks, which is related

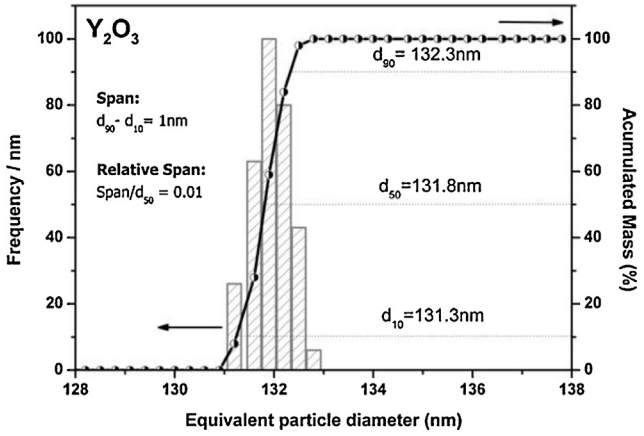

Fig. 2. Distribution of yttria equivalent particle diameter by PCS.

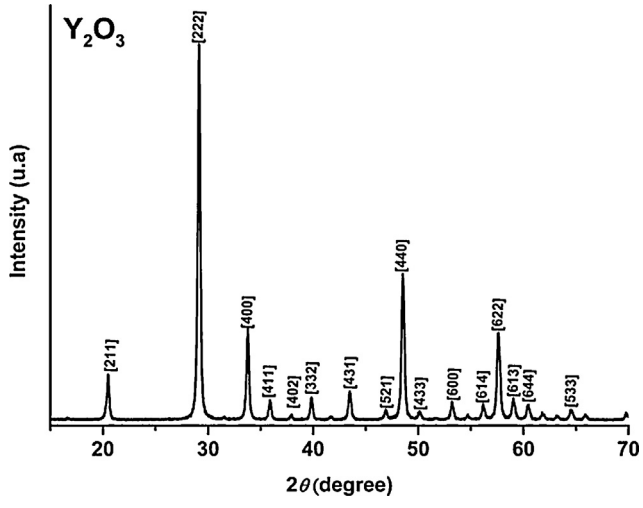

Fig. 3. Diffraction pattern of C-type cubic Y_2O_3 powders by X-ray diffraction (XRD) in accordance with PDF. 25-1200.

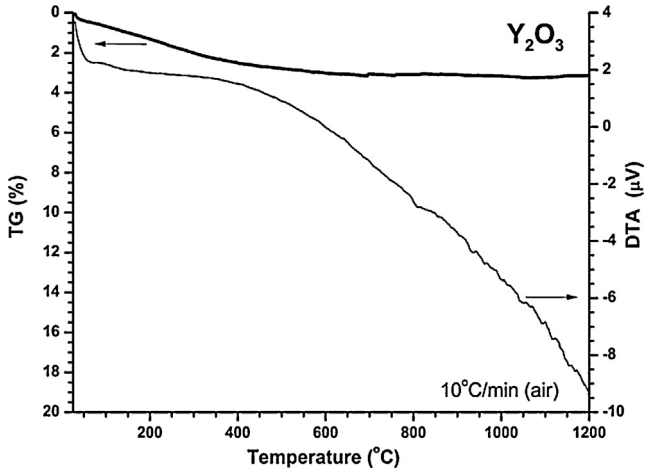

Fig. 4. TGA/TDA of Y_2O_3 powders at 10 °C/min until 1200 °C in ambient atmosphere.

Table 1
Particle characterization results of Y_2O_3 milled powders.

Specific surface area ($m^2\,g^{-1}$)	13.59
Real density ($g\,cm^{-3}$)	4.84
Calculated mean particle diameter (d_{BET}, nm)	91.20
Experimental mean particle diameter (d_{50}, nm)	131.80
Agglomeration factor – F_{ag}	1.45

to phase transformations was detected (narrow line). Besides, Y_2O_3 presents a loss of mass of 2.5 wt% due to particles dehydration (thick line).

Particle characterization results are summarized in Table 1. Specific surface area by BET method was 13.59 $m^2\,g^{-1}$. Real density corresponded to 94.90% of theoretical density (5.10 $g\,cm^{-3}$). Comparing calculated mean particle diameter (d_{BET}) from BET equation with experimental (d_{50}) from PCS the difference was only 40.6 nm. Further, the agglomeration factor (F_{ag}) was small 1.45, which means the particles were well dispersed.

Fig. 5 shows thermoluminescence (TL) spectra of yttria powders at heating hate of 10 °C/s from ambient temperature until 400 °C. From the figure the thermal stimulated emission spectra is composed by one peak (Fig. 5a), at 150 °C with the emission light quanta at λ = 550 nm. The major electron population which has been recombined by irradiation was thermal released from the traps within the material at 125 °C. The TL signal during exposure to the stimulation temperature is observed to decrease to a low level as the trapped charge is depleted above 125 °C (Fig. 5b). As predicted by TL theory,[24] the intensity of TL $I(t)$ in photons per second at any time (t) during heating is proportional to the rate of recombination of holes and electrons at potential role trap level (R). Consequently, TL intensity (I) can be defined as the derivative of the concentration of holes trapped (m) at (R), where the negative sign indicates a decrease of holes, as follows:

$$I(t) = -\frac{dm}{dt} \quad (4)$$

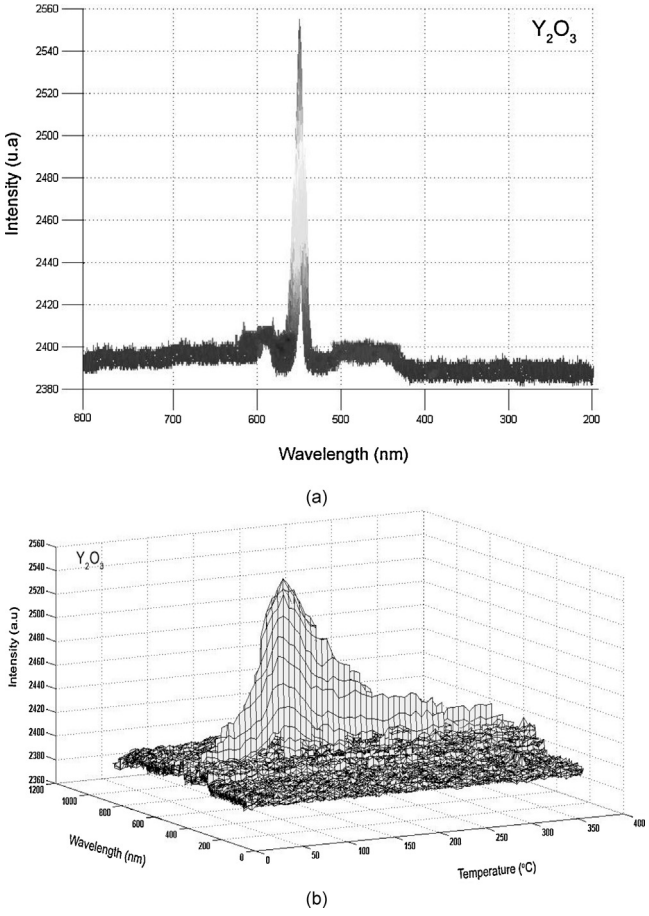

Fig. 5. TL emission spectra of yttrium oxide particles at heating rate of 5 °C/s until 400 °C. In (a) TL emission quanta at λ = 550 nm and (b) TL spectra as a function of wavelength and temperature, where TL emission at 150 °C.

Fig. 6 shows zeta potential curves of Y_2O_3 nanoparticles as a function of dispersant concentration and pH. According to[25] yttria particles are soluble in acid conditions, thus pH was set from 5.5 to 12.5. Suspensions with no dispersant (0 wt% PAA) presented an isoelectric point (IEP) at pH = 8.5. At this condition zeta potential is zero ($\zeta = 0$ mV), where attraction forces are very

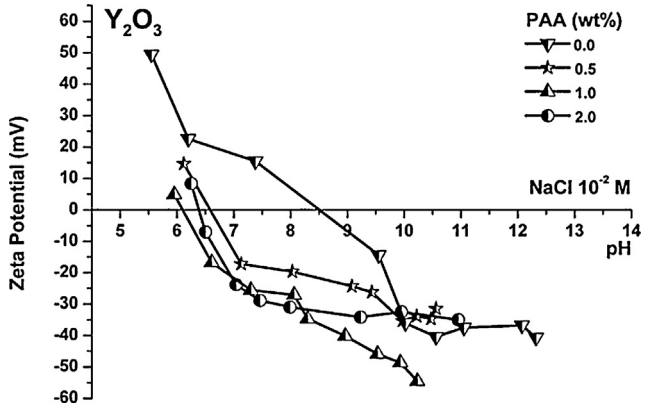

Fig. 6. Zeta potential curves of Y_2O_3 particles as a function of pH and dispersant (PAA, wt%) concentration.

strong and particles tend to agglomerate. Therefore, to prepare stable suspensions is desired to set up pH value far from IEP. For all pH range evaluated the stability of Y_2O_3 took place at pH < 7 ($|\zeta = 50$ mV|) and pH ≥ 9.5 ($|\zeta = 40$ mV|).

Using polyacrylic ammonium acid (PAA) as dispersant promotes stability of particles by electro steric mechanism. The prior interface liquid/particle surface changes to liquid/dispersant/particle surface. As a consequence zeta potential (ζ) and IEP are resulted from this interaction. PAA is based on carboxylic acid groups (COOH), in which dissociation mechanism is given as follows:

$$\text{A-COOH} + H_2O \leftrightarrow \text{A-COO}^- + H_3O^+ \quad (5)$$

According to the pH and ionic strength of the medium, the fraction of function groups that is dissociated (COO) and that which is not dissociated (COOH) will change. As the pH shifts from neutral to alkaline, the extent of dissociation and negative charge of the polymer increase. In addition, more negative charge adsorbs on the particles surface as well as polymer chains sketch. As a result, the stabilization of particles is improved by two ways, high charge of the polymer adsorbed on particle surface and the physical barrier by polymer chains sketched.

For all PAA concentrations IEP is displaced from pH = 8.5 to pH = 6 and pH = 6.5. Suspensions prepared with 0.5 wt% of PAA presented stable conditions at pH ≥ 7. For 1 wt% of PAA significant zeta potential values were achieved at pH ≥ 6.5 ($|\zeta \geq 20$ mV|), whereas for 2 wt% of PAA this condition is established at pH ≥ 6.7. Moreover the highest zeta potential, which means the best stability condition takes place at pH 10 ($|\zeta = 56$ mV|). The use of PAA as dispersant was useful to displace IEP to lower pH and to prepare stable suspensions apart from pH = 6.5. Based on these results, using 1 wt% of PAA and setting up pH = 10.5 were the best parameters to prepare highly stable suspensions. Based on these results, using 1 wt% of PAA and setting up pH = 10.5 ($|\zeta = 56$ mV|) were the most suitable parameters to prepare highly stable suspensions.

The correlation between zeta potential (ζ) and stability of particles in suspension is well understood when based on viscosity (η) results as shown in Fig. 7. For pH values beside IEP (pH = 8.5) result in low zeta potential ($\zeta < |5$ mV|), corresponding to weak dispersion (thin double electric layer), as well as higher viscosity. At pH = 8.8, ζ value is minimum ($|\zeta = 3.52$ mV|) whereas η is maximum (14 mPa s). On the other hand, shifting pH value to alkaline condition as pH = 10.5, ζ value is maximum ($|\zeta = 40$ mV|), whereas η is minimum (7 mPa s). Therefore, these results confirm those parameters from zeta potential curves, where pH = 10.5 supplied highly stable suspensions.

Fig. 8 shows the effectiveness of PAA on stability of Y_2O_3 suspensions prepared with 25 vol% of solids, pH = 10.5 and based on a shear rate of 500 s^{-1}. Considering all PAA concentrations (0–2 wt%) suspensions prepared with no PAA (0 wt%) presented highest viscosity (70 mPa s). In contrast by using PAA a significant decrease of viscosity was promoted. For PAA = 0.5 wt% η decreased from 70 mPa s to 25 mPa s whereas

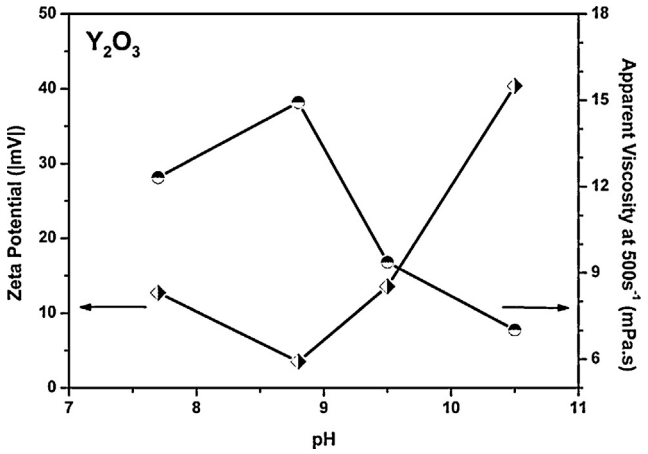

Fig. 7. Correlation between zeta potential (ζ) and apparent viscosity (η, 500 s^{-1}) for Y_2O_3 suspensions.

PAA = 1.0 wt% η = 10 mPa s. Nevertheless the efficiency in dispersing particles was not found at PAA = 2 wt%. Indeed, a tendency to increase ionic strength of medium and consequently reduction of interparticle dispersion forces was observed. Thus, PAA = 1 wt% was defined as the suitable concentration for dispersant dosage.

Afterwards evaluating and defining stability parameters (pH and dispersant dosage), the flow behavior of Y_2O_3 suspensions was appraised by control rate curves (CR) as shown in Fig. 9. As a consequence of solids load suspensions those with 25 vol% showed linear flow (both up and down curves) fitting to Newtonian model.[18] However, increasing to 30 vol% flow behavior changed from linear to dilatant flow, where the viscosity (η) increases according to shear stress (τ) applied. Dilatant behavior is due to overlapping of electric double layers of particles (in a high solids load condition) when subjected to external forces. As a result strong a repulsion forces between particles occurs and the viscosity increases. In this condition the flow behavior of suspension fitted to Oswald de Walle model.[18] Moreover, suspensions with 33 vol% behave like dilatant flow, showing a

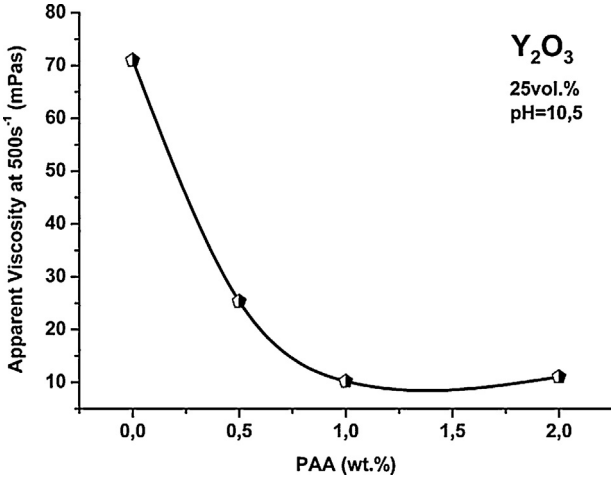

Fig. 8. Effectiveness of PAA on stability of Y_2O_3 suspensions with 25 vol%.

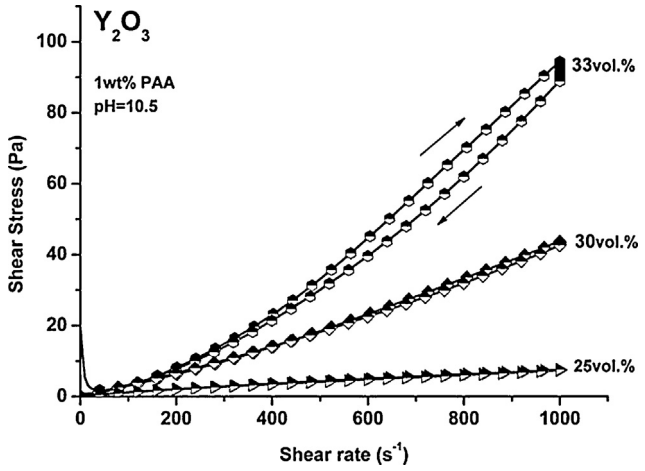

Fig. 9. CR flow curves of Y_2O_3 suspensions with solids load from 25 to 33 vol%, PAA = 1 wt% and pH 10.5.

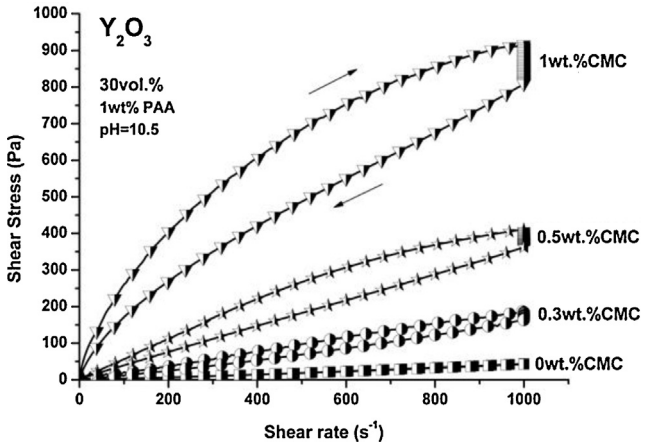

Fig. 11. CR flow curves of Y_2O_3 suspensions with 30 vol% as a function of CMC concentration from 0 to 1 wt%.

maximum shear stress of 98 Pa at 1000 s^{-1}. For replica method dilatant suspensions are not desired seeing that they show higher viscosity when subjected to shearing during the immersion of template into suspension. Likewise, considering templates based on complex morphology dilatant suspensions are not suitable to be applied in replica processing.

Yttria suspensions with up to 25 vol% of particles presented low viscosity ($\eta < 10$ mPa s), which usually supplies linear flow behavior as indicated in Fig. 10. However, increasing to 30 vol% η shifted from 9 mPa s to 37 mPa s, which was a significant difference. High solid suspensions tend to have high viscous flow, considering the space between particles is shorter and as consequence, the effect of interparticle forces is more intense. Moreover, for suspensions with 33 vol% of particles viscosity was maximum ($\eta = 66$ mPa s). It was due to the overlapping of electro-steric layers of particles supplied by HTMA and PAA, which results in strong repulsion between particles. This condition supplied dilatant behavior.

Fig. 11 shows flow curves of Y_2O_3 suspensions with 30 vol% of solids and CMC concentration from 0 to 1 wt% (weight percent, wt%). The suspension prepared with no CMC presented linear flow, fitting to Newtonian model. On the other hand, using CMC changed flow behavior from linear to shear thinning. Besides, an area between up and down curves was formed apart from 0.3 wt% of CMC. This behavior, known as thixotropy is related to the condition of suspended particles. Based on up curves (from 0 to 1000 s^{-1}) agglomerated particles structures (APS) formed by CMC long chains were broken down in smaller sizes, afterwards particles were dispersed and realigned. As a result, at 1000 s^{-1} and for a determined time the viscosity decreases to a minimum value. As soon as the shear stress starts decreasing (beginning of down curve, from 1000 to 0 s^{-1}) APS tends to recover its initial state and an area between up and down curves was formed. In addition, the most APS was formed with 1 wt% of CMC (164 Pa s^{-1}).

Fig. 12 shows the thermo gravimetric analyze (TGA) result of CNT template. Up to 250 °C a slight loss of weight occurred around 4 wt%. However, a large loss of weight around 76 wt% was observed in the range from 251 °C to 350 °C. Apart from 315 °C the loss of weight still went on, where at 600 °C CNT template was totally eliminated (100 wt%). Based on these

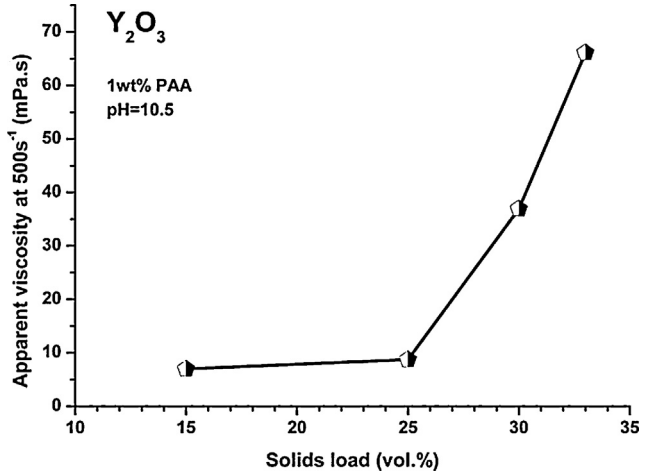

Fig. 10. Variation of apparent viscosity of Y_2O_3 suspensions as a function of solids load from 15 to 33 vol%.

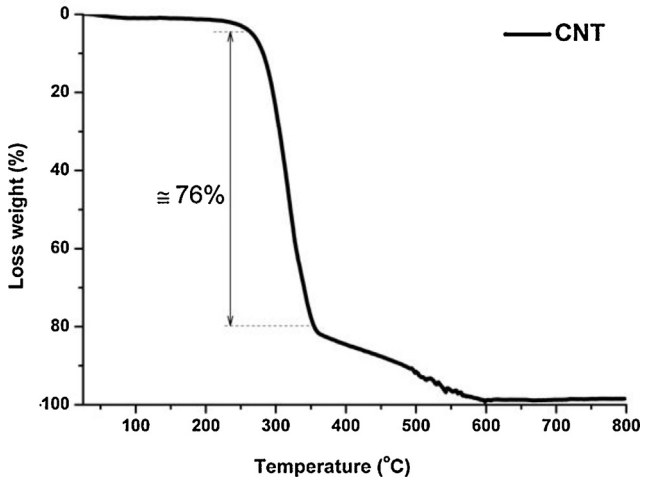

Fig. 12. ATG of CNT template at 10 °C/min, 800 °C in air.

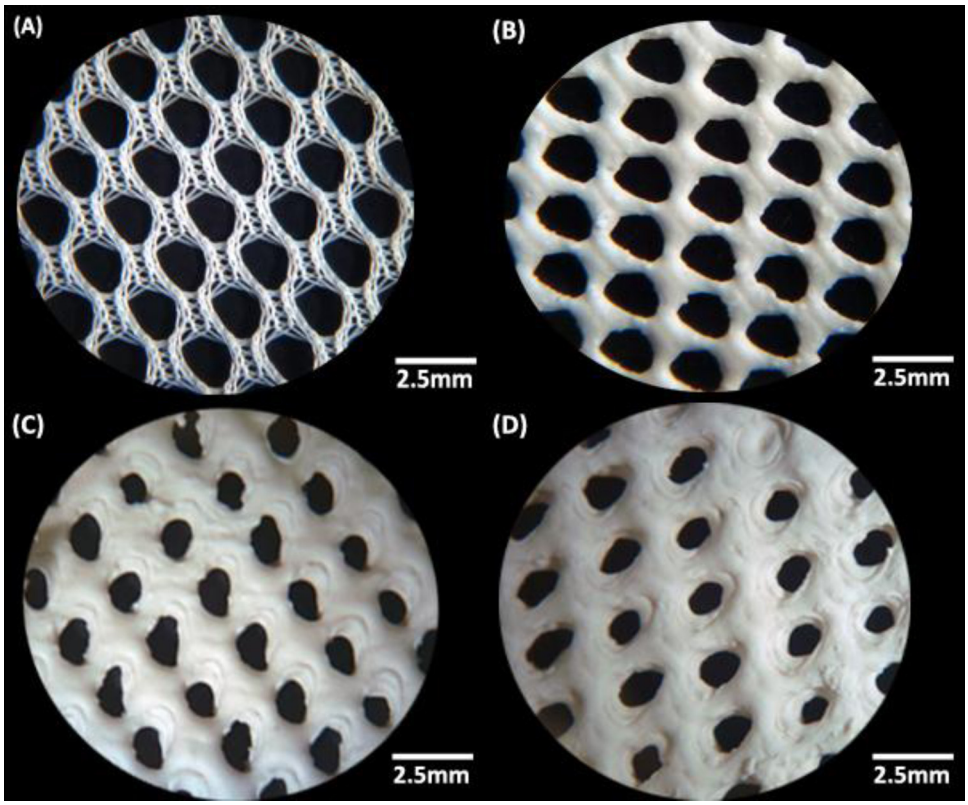

Fig. 13. Sintered ceramic nettings impregnated with yttria suspensions prepared with CMC concentrations from 0.3 to 1 wt%. In (A) replica template; (B) CMC = 0.3 wt%, (C) CMC = 0.5 wt% and (D) CMC = 1.0 wt%.

results, the following thermal treatment condition for impregnated templates (temperature/time) was set as 1600 °C/1 h with heating rate at 1 °C/min.

Fig. 13 shows sintered Y_2O_3 replicas based on suspensions prepared with 30 vol%, pH = 10.5 and CMC from 0.3 wt% to 1 wt%. Samples impregnated into suspensions with 0.5 wt% and 1 wt% of CMC and sintered showed high density 4.79 g cm^{-3} and 4.83 g cm^{-3} respectively, and thick struts, heterogeneous cells and rough surface. Besides suspensions prepared with 0.3 wt% of CMC resulted in replicas near template shape, homogeneous distribution of cells (size and morphology) and density of 4.25 g cm^{-3}, which corresponds to 85% of theoretical density. The overall performance of porous burners will depend on the combination of material and porous structure. Compared with most commonly used ceramics such as alumina (Al_2O_3),[26] silicon carbide (SiC)[27] and zirconia (ZrO_2),[28] yttria presents unique luminescence proprieties due to its chemical and physical similarity with rare earth elements. Besides, yttria shows other useful proprieties for porous burners applications as thermal conductivity, emissivity, temperature and corrosion resistance, thermal expansion and mechanical strength at high temperatures. Fig. 14 shows the microstructure of sintered samples, which consists in heterogeneous distribution porous and grains with size smaller than 3 μm. Porosity is also an important parameter, since it determines convective heat transport, flame stability and combustion effectiveness of the porous burner. Sintered replicas showed mechanical strength, which is suitable for handling. Some studies have been shown the low mechanical strength of components produced by replica method.[29,30] However, this problem can be mitigated by controlling suspension structure via stability of particles and thermal treatment of impregnated samples. Table 2 summarizes rheological parameters from Y_2O_3 suspension based on CR flow curves. The following results confirm that equilibrium between thixotropy and viscosity is essential in order to impregnate porous templates.

Table 2
The best processing parameters by rheology of Y_2O_3 suspensions for replica method.

Solids load (vol%)	pH	Binder (wt%)	η (mPa s)	τ (Pa)	Thixotropy (Pa s^{-1})
30.0	10.5	0.3	424.0	42.49	7.435

η, apparent viscosity at 100 s^{-1}.

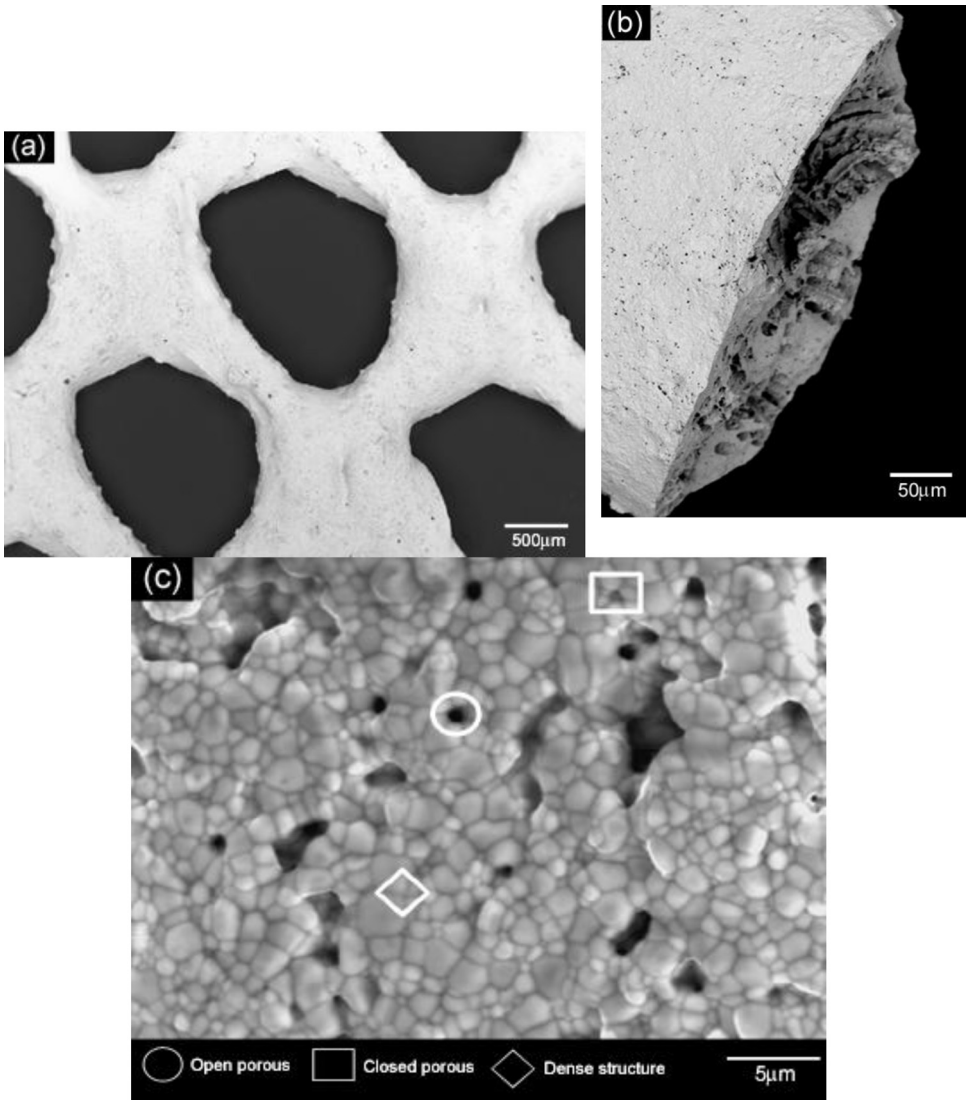

Fig. 14. Microstructure of yttria nettings produced by immersion into suspension with 0.3 wt% of CMC and sintered at 1600 °C/1 h.

4. Conclusion

By colloidal processing of yttria ceramic nettings with homogeneous cells and struts were produced by replica method. Yttria nanoparticles ($d_{50} = 138.50$ nm) presented luminescence light emission with $\lambda = 550$ nm when being thermal stimulated at 150 °C with heating rate of 5 °C/s. Besides yttria nanoparticles were highly stable at pH 10.5 and adding 1 wt% of ammonium poly-acrylic acid ($|\zeta = 56$ mV|). By rheological analyzes yttria suspensions with 30 vol% of solids, pH 10.5, 1 wt% of dispersant and 0.3 wt% of carboximetilcelulose presented flow behavior, thixotropy and viscosity suitable for replica method. As result, ceramic nettings sintered at 1600 °C/1 h in environmental atmosphere showed mechanical strength and porous microstructure, which is essential to supply convective heat transport, flame stability and combustion effectiveness of the porous burner.

Acknowledgements

We authors are deeply thankful for Dr. Linda Caldas and Dr. Maira Tiemi Yoshizumi to help us with thermoluminescence characterization of yttria powders. São Paulo Research Foundation (FAPESP), National Council for Scientific and Technological Development (CNPq) and Coordination of Improvement of High Degree People (CAPES) for financial scholarship support of the student Silas Cardoso dos Santos.

References

1. Hoekstra HR, Gingerich KA. High-pressure B-type polymorphs of some rare-earth sesquioxides. *Science* 1964;**146**:1163.
2. Gourlaouen V, Schnedecker G, Lejus AM, Boncoeur M, Collongues R. Metastable phases in yttrium-oxide plasma spray deposits and their effect on coating properties. *Mater Res Bull* 1993;**28**:415–25.

3. Navrotsky A, Benoist L, Lefebvre H. Direct calorimetric measurement of enthalpies of phase transitions at 2000 degrees–2400 degrees C in yttria and zirconia. *J Am Ceram Soc* 2005;**88**:2942–4.
4. Qin X, Ju YG, Bernhard S, Yao N. Flame synthesis of Y_2O_3: Eu nanophosphors using ethanol as precursor solvents. *J Mater Res* 2005;**20**:2960–8.
5. Wang WN, Widiyastuti W, Ogi T, Lenggoro IW, Okuyama K. Correlations between crystallite/particle size and photoluminescence properties of submicrometer phosphors. *Chem Mater* 2007;**19**:1723–30.
6. Zhang H, Cen Y, Chen LF, Zhu HY, Qian LJ, Fan DY. Full-angle collimations of two-dimensional photonic crystals with ultrahigh-index background materials. *J Opt-Uk* 2010;**12**.
7. Goldburt ET, Kulkarni B, Bhargava RN, Taylor J, Libera M. Size dependent efficiency in Tb doped Y_2O_3 nanocrystalline phosphor. *J Lumin* 1997;**72–74**:190–2.
8. Barrer RM, White EAD. Contributions to the hydrothermal chemistry of silicates 1. *Chem Ind (London)* 1951:146–7.
9. Ki-moon B. Energy for a sustainable future. In: *Summary report and recomendations, United Nations.*; 2010.
10. Studart AR, Gonzenbach UT, Tervoort E, Gauckler LJ. Processing routes to macroporous ceramics: a review. *J Am Ceram Soc* 2006;**89**:1771–89.
11. Liu ZT, Fan TX, Zhang W, Zhang D. The synthesis of hierarchical porous iron oxide with wood templates. *Microporous Mesoporous Mater* 2005;**85**:82–8.
12. Sherman AJ, Tuffias RH, Kaplan RB. Refractory ceramic foams – a novel, new high-temperature structure. *Am Ceram Soc Bull* 1991;**70**:1025–9.
13. Luyten J, Thijs I, Vandermeulen W, Mullens S, Wallaeys B, Mortelmans R. Strong ceramic foams from polyurethane templates. *Adv Appl Ceram* 2005;**104**:4–8.
14. Silva SA, Brunelli DD, Melo FCL, Thim GP. Preparation of a reticulated ceramic using vegetal sponge as templating. *Ceram Int* 2009;**35**: 1575–9.
15. Ben-Nissan B. Natural bioceramics: from coral to bone and beyond. *Curr Opin Solid State Mater Sci* 2003;**7**:283–8.
16. Roy DM, Linnehan SK. Hydroxyapatite formed from coral skeletal carbonate by hydrothermal exchange. *Nature* 1974;**247**:220–2.
17. White RA, White EW, Weber JN. Replamineform – new process for preparing porous ceramic, metal, and polymer prosthetic materials. *Science* 1972;**176**:922.
18. Moreno R. *Reología de suspensiones cerámicas*. Madrid: Consejo Superior de Investigaciones Científicas; 2005.
19. Moreno R, Salomoni A, Mello Castanho S. Colloidal filtration of silicon nitride aqueous slips. Part I: Optimization of the slip parameters. *J Eur Ceram Soc* 1998;**18**:405–16.
20. Fuji M, Kato T, Zhang FZ, Takahashi M. Effects of surfactants on the microstructure and some intrinsic properties of porous building ceramics fabricated by gelcasting. *Ceram Int* 2006;**32**:797–802.
21. Li X, Li Q. YAG ceramic processed by slip casting via aqueous slurries. *Ceram Int* 2008;**34**:397–401.
22. Sonoda K, Higashi K, Ono H, Sameshima S, Hirata Y. Surface properties and aqueous processing of rare earth-doped ceria powders by coprecipitation method. *Novel Synth Process Ceram* 1999;**159–160**:169–74.
23. Santos SC. Processamento coloidal de componentes cerâmicos para queimadores de gás. In: *Instituto de Pesquisas Energéticas e Nucleares (IPEN)*. 2010. p. 73.
24. Weigelt C, Aneziris CG, Yanina A, Guk S. Ceramic processing for TRIP-steel/Mg-PSZ composite materials for mechanical applications. *Steel Res Int* 2011;**82**:1080–6.
25. Sprycha R, Jablonski J, Matijević E. Zeta potential and surface charge of monodispersed colloidal yttrium (III) oxide and basic carbonate. *J Colloid Interface Sci* 1991;**149**:562–8.
26. Saleh HI. Preparation and characterisation of Sb_2O_3 with or without Cr_2O_3 and CoO containing ZnO varistors. *Br Ceram Trans* 2004;**103**:171–5.
27. Ananthakumar S, Manohar P, Warrier KGK. Effect of boehmite and organic binders on extrusion of alumina. *Ceram Int* 2004;**30**:837–42.
28. Gomez SY, Escobar JA, Alvarez OA, Rambo CR, de Oliveira APN, Hotza D. ZrO_2 foams for porous radiant burners. *J Mater Sci* 2009;**44**:3466–71.
29. Luyten J, Mullens S, Cooymans J, De Wilde AM, Thijs I, Kemps R. Different methods to synthesize ceramic foams. *J Eur Ceram Soc* 2009;**29**:829–32.
30. Saggiowoyansky J, Scott CE, Minnear WP. Processing of porous ceramics. *Am Ceram Soc Bull* 1992;**71**:1674–82.